© 2015. Published by The Company of Biologists Ltd | Journal of Cell Science (2015) 128, 1627–1638 doi:10.1242/jcs.163105

RESEARCH ARTICLE

Transbilayer distribution of lipids at nano scale

Motohide Murate[1], Mitsuhiro Abe[1], Kohji Kasahara[2], Kazuhisa Iwabuchi[3], Masato Umeda[4] and Toshihide Kobayashi[1,5,*]

ABSTRACT

There is a limited number of methods to examine transbilayer lipid distribution in biomembranes. We employed freeze-fracture replica-labelling immunoelectron microscopy in combination with lipid-binding proteins and a peptide to examine both transbilayer distribution and lateral distribution of various phospholipids in mammalian cells. Our results indicate that phospholipids are exclusively distributed either in the outer or inner leaflet of human red blood cell (RBC) membranes. In contrast, in nucleated cells, such as human skin fibroblasts and neutrophils, sphingomyelin was distributed in both leaflets while exhibiting characteristic lipid domains in the inner leaflet. Similar to RBCs, lipid asymmetry was maintained both in resting and thrombin-activated platelets. However, the microparticles released from thrombin-activated platelets lost membrane asymmetry. Our results suggest that the microparticles were shed from platelet plasma membrane domains enriched with phosphatidylserine and/or phosphatidylinositol at the outer leaflet. These findings underscore the strict regulation and cell-type specificity of lipid asymmetry in the plasma membrane.

KEY WORDS: Plasma membrane, Lipid asymmetry, Microdomain, Electron microscopy, Freeze fracture

INTRODUCTION

The asymmetric distribution of lipids between the outer and inner leaflet of the membrane bilayer was first reported in red blood cells (RBCs) (Bretscher, 1972a; Bretscher, 1972b; Gordesky et al., 1972; Verkleij et al., 1973). Using membrane-impermeable reagents that covalently bind to the lipid headgroup (Bretscher, 1972a; Bretscher, 1972b; Gordesky et al., 1972) or by selectively degrading the outer-leaflet phospholipids with specific phospholipases (Bütikofer et al., 1990; van Meer et al., 1981; Verkleij et al., 1973), it has been shown that 65–75% of phosphatidylcholine (PC) and ~80% of sphingomyelin (SM) are located in the outer leaflet, whereas 80–85% of phosphatidylethanolamine (PE), over 96% of phosphatidylserine (PS) and 80% of phosphatidylinositol 4,5-bisphosphate (PIP_2) are located in the inner leaflet of the human RBC membrane (Devaux, 1991; Zachowski, 1993).

[1]Lipid Biology Laboratory, RIKEN, Wako, Saitama 351-0198, Japan. [2]Laboratory of Biomembrane, Tokyo Metropolitan Institute of Medical Science, Setagaya-ku, Tokyo 156-8506, Japan. [3]Laboratory for Biochemistry, Institute for Environmental and Gender-specific Medicine, Juntendo University Graduate School of Medicine, Urayasu, Chiba 279-0021, Japan. [4]Department of Synthetic Chemistry and Biological Chemistry, Graduate School of Engineering, Kyoto University, Nishikyo-ku, Kyoto 615-8510, Japan. [5]Institut National de la Santé et de la Recherche Médicale (INSERM) Unité 1060, Université Lyon 1, Villeurbanne 69621, France.

*Author for correspondence kobayasi@riken.jp

Received 10 September 2014; Accepted 2 February 2015

Although these experiments have been crucial in elucidating the important concept of lipid asymmetry, there are several limitations. The methods require a relatively long incubation time (10–120 min) and do not account for the possibility of lipid re-organisation during the course of the treatment. In addition, these methods are, in principle, best for single-membrane system, such as RBCs (Bretscher, 1972a; Bütikofer et al., 1990; Gordesky et al., 1972; van Meer et al., 1981; Verkleij et al., 1973) and gram-positive bacteria (Rothman and Kennedy, 1977). Application of these methods to multi-membrane systems, such as eukaryotic cell membranes, requires additional measures in order to obtain highly purified membrane preparations (Chap et al., 1977; Perret et al., 1979; Post et al., 1988; Record et al., 1984; Schick et al., 1976).

In sodium dodecyl sulphate (SDS)-digested freeze-fracture replica labelling (FRL), hereafter referred to as SDS-FRL, cells are quickly frozen (in less than 50 msec) (Ryan et al., 1990), and the outer- and the inner-leaflet monolayers are separated. During freeze-fracture sample preparation, lipids and proteins are fixed on thin metal cast. SDS treatment is necessary to remove unfractured membranes and cytoplasmic components, and also to prime the membranes for specific probes. It has been reported that at least 70% of PC in the replica remains after SDS treatment (Fujimoto et al., 1996); and Fujita and Fujimoto obtained a similar result (Fujita and Fujimoto, 2007). In theory, this method is applicable to any cells and tissues, although sometimes it is difficult to identify the membrane of interest. Quick freezing of the specimen and physical fixation are expected to minimise re-organisation of the lipids during sample preparation. SDS-FRL, therefore, provides a suitable method to examine lipid asymmetry in different specimens. Indeed, this method has been applied to study the transbilayer distribution of PC (Fujimoto et al., 1996) by using a specific monoclonal anti-PC antibody. It was demonstrated that, unlike previous biochemical studies, PC is exclusively distributed in the outer leaflet of the RBC membrane.

The difficulty of obtaining effective and selective lipid-binding probes, however, hindered further application of this method. The recent development of peptides and proteins that recognise specific lipids or lipid clusters has made it possible to apply SDS-FRL to a systematic analysis of both lateral and transbilayer lipid distribution (Fujita et al., 2007; Fujita et al., 2009b; Murate et al., 2010). Since lipids are indirectly detected by the lipid probes, careful experiments are required to obtain a conclusion in the lipid detection of SDS-FRL. Particularly, the possibility of a multiple-binding secondary antibody is a problem. However, previous experiments by Fujita et al. (Fujita et al., 2007) demonstrated that multivalent gold-labelled secondary antibody and monovalent gold-labelled protein A gave very similar results after appropriate statistical analysis. Until now, successful experiments identified the lateral distribution of ganglioside,

Journal of Cell Science (2015) 128, 1627–1638 doi:10.1242/jcs.163105

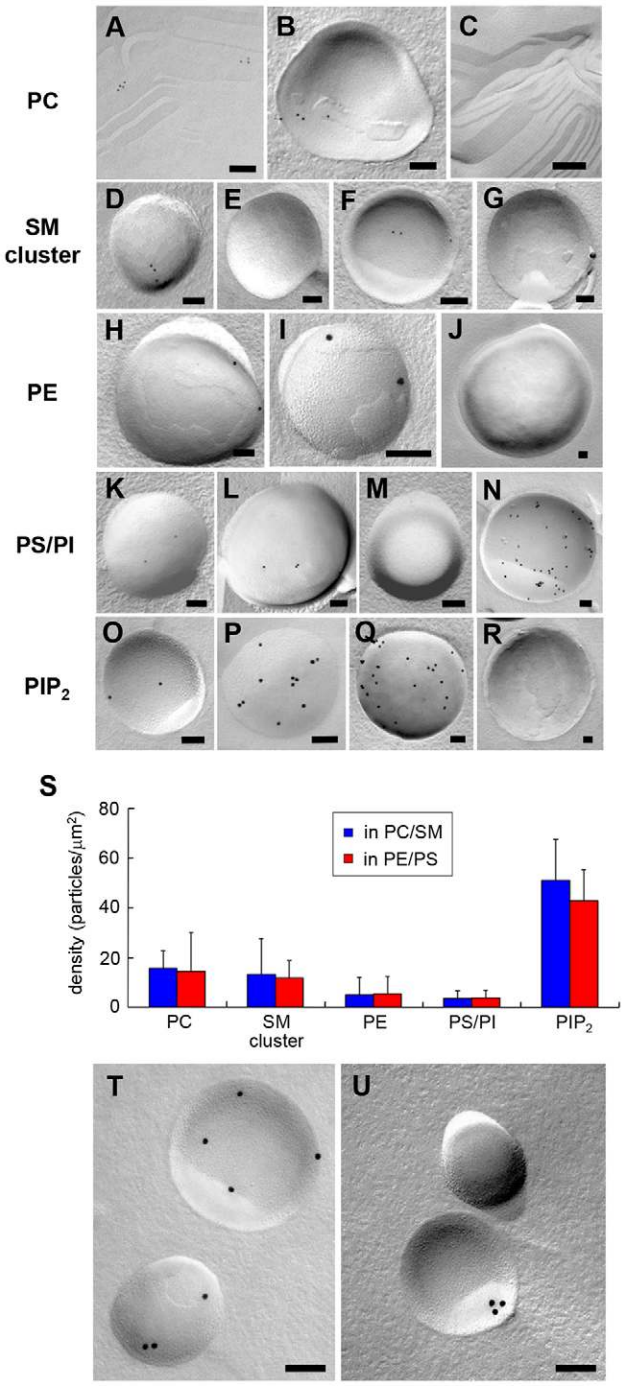

Fig. 1. Binding specificity of lipid probes to model membranes. Binding of anti-PC antibody to model membrane composed of: (A) POPC:egg SM (1:99), (B) POPC:POPE:POPS (1:49.5:49.5), (C) POPS:egg SM (1:99). Binding of MBP–lysenin to liposomes composed of: (D) egg SM:POPC (1:99), (E) egg SM:POPE:POPS (1:49.5:49.5), (F) egg SM:DOPE:POPS (1:49.5:49.5), (G) POPS:POPC (1:99). Binding of biotinylated duramycin to: (H) POPE:POPC (1:99), (I) POPE:POPS (1:99), (J) POPS:POPC (1:99). Binding of anti-PS antibody (clone 1H6) to model membrane composed of: (K) POPS:POPC (1:99), (L) POPS:POPE (1:99), (M) POPE:POPC (1:99), (N) liver PI:POPC (1:9). Binding of anti-PIP_2 antibody to liposomes of: (O) brain PIP_2:POPC (0.1:99.9), (P) brain PIP_2:POPC (1:99), (Q) brain PIP_2:POPE:POPS (1:49.5:49.5), (R) POPS:POPC (1:99). (S) Quantification of labelling densities of the probes in membranes with different lipid composition. The number of gold particles per μm^2 was compared to those in membranes with different lipid composition (mean±s.d.). No significant differences were detected across the membranes ($P>0.2$, Mann–Whitney U test). In each case, more than six randomly selected areas were analysed. (T) Distribution of gold particles after incubation of biotinylated duramycin using symmetric liposomes composed of lyso-PE:POPC:cholesterol (10:45:45). Scale bars: 100 nm. (U) Distribution of gold particles together with asymmetric liposomes that had been prepared as described in Materials and Methods.

monosialoganglioside (GM1), trisialotetrahexosylganglioside (GM3) (Fujita et al., 2007) and the recently identified phosphatidylglucoside on the outer leaflet (Murate et al., 2010) and PIP_2 in the inner leaflet of the plasma membrane in cultured cells (Fujita et al., 2009b).

In this study, we measured the transbilayer and the lateral distribution of lipids in several samples, including the membrane of human RBCs, and plasma membrane of human skin fibroblasts (HSFs), HeLa cells, neutrophils and platelets, by using the SDS-FRL method, and a combination of one peptide and various proteins that selectively bind to specific lipids and/or lipid clusters. Our results indicate that, in contrast to previous biochemical analysis, each lipid is almost exclusively distributed to either the outer or inner leaflet of RBC membranes. In contrast to RBCs, a substantial number of SM clusters distributed in the inner leaflet of HSFs and neutrophil plasma membranes, where they form distinct lipid domains. A brief activation of platelets by using thrombin did not alter the asymmetric distribution of phospholipids of the plasma membrane, whereas the platelet-shed microparticles lost asymmetry. Our experiments suggest that the microparticles are released from the specific plasma membrane domains of platelets, where PS and/or phosphatidylinositol (PI) were exposed to the outer leaflet. These results underscore that the asymmetric distribution of lipids in the plasma membrane is strictly regulated and cell-type specific.

RESULTS

Specificity and sensitivity of the lipid probes used in the SDS-FRL method

Since lipid detection using SDS-FRL primarily depends on the specificity and sensitivity of the lipid probes, we first characterised our lipid probes by using model membranes with a defined lipid composition. To study the transbilayer distribution of lipids, it is crucial to ensure the labelling efficiency of the lipids is the same between the extracellular surface and the protoplasmic surface. In this study we measured the binding of various lipid probes to model membranes that resemble the outer leaflet containing PC and/or SM (PC/SM) and inner leaflet containing PE and/or PS (PE/PS) of the plasma membrane.

To detect PC, we employed a monoclonal antibody that specifically binds to PC (Fujimoto et al., 1996; Nam et al., 1990), followed by a colloidal gold-labelled secondary antibody. The anti-PC antibody does not bind to other phospholipids, including SM, which shares the phosphocholine moiety with PC (Nam et al., 1990). The specific binding of this antibody to PC was confirmed with SDS-FRL method using model membranes. The gold particles were detected in membranes containing PC:SM (Fig. 1A) as well as PC, PE and PS (PC:PE:PS) (Fig. 1B), but not in the membranes containing PS and SM (PS:SM) (Fig. 1C). In Fig. 1A, gold particles accumulated in specific domains, indicating the phase separation of PC and SM (Ishitsuka et al., 2004). Fig. 1A,B demonstrates that, even at a low PC content 1% (mol/mol), the antibody binds similarly to the model membranes

Journal of Cell Science

Journal of Cell Science (2015) 128, 1627–1638 doi:10.1242/jcs.163105

that mimic outer- or inner-leaflet lipid environment (summarised in Fig. 1S).

SM was detected by using the maltose-binding protein (MBP)-tagged lysenin (MBP–lysenin) (Kiyokawa et al., 2005) followed by an anti-MBP antibody and a colloidal gold-labelled secondary antibody. Lysenin binds to SM only when the lipid forms clusters of five to six molecules (Ishitsuka et al., 2004) that are dependent on the miscibility of SM to the other lipids. Please notice that we use 'cluster' when referring to small aggregates composed of few molecules, and 'domain' when referring to the specific area of the membrane that accumulates immunogold labelling. Fig. 1D,E indicate that MBP–lysenin labelled SM in 1-palmitoyl-2-oleoyl-*sn*-glycero-3-phosphocholine (POPC) but not in 1-palmitoyl-2-oleoyl-*sn*-glycero-3-phosphoethanolamine (POPE):1-palmitoyl-2-oleoyl-*sn*-glycero-3-phospho-L-serine (POPS). This may be due to the differences in miscibility of chicken egg-derived SM (egg SM) with POPC and POPE:POPS. The gel-to-liquid crystalline phase transition temperature of N-palmitoyl-D-*erythro*-sphingosylphosphorylcholine, the predominant component of egg SM, is around 41℃, and of POPC is −4℃ (Marsh, 2013). The big difference of the transition temperatures induces phase separation and clustering of SM. In contrast, the transition temperatures of POPE and POPS are 26℃ and 14℃, respectively (Marsh, 2013). An egg SM transition temperature that is closer to that of POPE than of POPC increases the miscibility of SM in membranes that contain POPE and POPS (POPE:POPS) and decreases the number and sizes of SM clusters. Indeed, changing POPE to fluid 1,2-dioleoyl-*sn*-glycero-3-phosphoethanolamine (DOPE), whose transition temperature is −8℃ (Marsh, 2013), resulted in binding of MBP–lysenin to liposomes (Fig. 1F). MBP–lysenin did not bind to PS:PC (1:99) liposomes (Fig. 1G). In the following experiments, we employed MBP–lysenin as an SM-cluster-binding probe.

Wild type lysenin oligomerises to form a pore within the membrane after binding to SM and is, therefore, cytotoxic (Ishitsuka and Kobayashi, 2007; Yamaji-Hasegawa et al., 2003; Yilmaz et al., 2013). Similar to wild type lysenin, MBP–lysenin is haemolytic (Kiyokawa et al., 2004), suggesting that oligomerisation of the protein occurs in the presence of SM. Oligomerisation of the protein may result in false-positive immunogold aggregates. Although lipids are physically fixed on the carbon and platinum replicas in SDS-FRL (Fujimoto et al., 1996; Fujita and Fujimoto, 2007) and the addition of polyvalent anti-lipid IgM antibody did not lead to immunogold aggregates in a previous study (Fujita et al., 2007), it was important to examine whether the employment of MBP–lysenin results in artificial aggregation of gold particles under our experimental conditions. To study this possibility, we labelled SM:PC (99:1) membranes with MBP–lysenin, followed by anti-MBP antibody and gold-conjugated secondary antibody (supplementary material Fig. S1A as a representative). Because of the high concentration of SM, immunogold aggregates should not be detected unless artificially induced by MBP–lysenin. The gold patterns were analysed using Ripley's K-function (Haase, 1995; Kiskowski et al., 2009; Perry, 2004; Ripley, 1979). The L(r)-r values indicated a random distribution within all specimens ($n=10$) (supplementary material Fig. S1B). This result suggests that the aggregation of the lipids on replicated cast was not induced by the application of probes in our experimental conditions, and that multivalent binding of anti-MBP and gold-labelled secondary antibodies did not affect the cluster analyses of gold particles. Fujita and colleagues also demonstrated that IgM antibody against ganglioside GM3 did not induce artificial clustering of the lipid (Fujita et al., 2007).

PE was visualised with biotinylated duramycin (Iwamoto et al., 2007), followed by a colloidal gold-conjugated anti-biotin antibody. Duramycin is a 19-amino-acid tetracyclic peptide that specifically binds to PE (Iwamoto et al., 2007; Rzeźnicka et al., 2010). Duramycin is a single-amino-acid variant of cinnamycin (Iwamoto et al., 2007; Rzeźnicka et al., 2010) that is reported to form an equimolar complex with PE (Hosoda et al., 1996). Fig. 1H,I,S that duramycin detects 1% (mol/mol) PE in the PC (Fig. 1H) and PS membranes (Fig. 1I). Crossreaction to PS was not detected (Fig. 1J).

Lactadherin C2 domain (Lact-C2) has been employed to label PS of living cells (Yeung et al., 2008). When the specimen of 1% (mol/mol) of PS in PC liposomes was treated with polyhistidine-tagged Lact-C2 (His-Lact-C2), followed by anti-polyhistidine antibody and a colloidal gold-conjugated secondary antibody, distinctive gold particles were seen not only in liposomes, but also in replica membranes outside liposomes (supplementary material Fig. S2A). This result indicated that lactadherin is not suitable in SDS-FRL. We also tried anti-PS antibody (clone PS4A7) (Umeda et al., 1989), followed by a gold-conjugated secondary antibody. This antibody bound specifically to PS 1% (mol/mol) in PC liposomes (supplementary material Fig. S2B), but signals were also observed in PE:PC (1:99) liposomes (supplementary material Fig. S2C). We then examined another antibody against PS (clone 1H6), which gave analogous positive signals when 1% (mol/mol) of PS was added to PC (Fig. 1K) or in PE liposomes (Fig. 1L,S). Unlike clone PS4A7, this antibody did not bind to PE:PC (1:99) liposomes (Fig. 1M). It has previously been reported that, using lipid-coated beads, this antibody also binds PI and phosphatidic acid (PA), albeit to a lesser degree (Yeung et al., 2009). By using the SDS-FRL method, we confirmed that the 1H6 antibody bound to PI at a concentration of 10% (mol/mol) in PC liposomes (Fig. 1N), whereas no binding was observed in 10% (mol/mol) PA in PC liposomes (supplementary material Fig. S2D). In the following experiments, we employed clone 1H6 of the anti-PS antibody as a PS/PI-binding probe.

Localisation of PIP_2 was determined by using an anti-PIP_2 monoclonal antibody (Miyazawa et al., 1988), followed by a colloidal gold-labelled secondary antibody. Previously, it has been shown that this antibody recognised PIP_2 but not phosphatidylinositol-4-monophosphate or other negatively charged phospholipids (Miyazawa et al., 1988). This antibody detected PIP_2 at a concentration as low as 0.1% (mol/mol) in PC liposomes (Fig. 1O). In addition, the antibody bound to PIP_2:PC (1:99) (Fig. 1P) and PIP_2:PE:PS (1:49.5:49.5) (Fig. 1Q,S) similarly, but not to PS:PC (1:99) liposomes (Fig. 1R).

To verify whether our fixation protocol affect asymmetric distribution of lipids, we next examined lipid distribution in asymmetric liposomes using SDS-FRL. Asymmetric liposomes were prepared by incubating PC:cholesterol (1:1) liposomes with 10% (mol/mol) 1-palmitoyl-2-hydroxy-*sn*-glycero-3-phosphoethanolamine (lyso-PE). We also prepared symmetric liposomes in which lyso-PE was mixed with PC:cholesterol before preparation of liposomes. Previously we showed that duramycin binds both PE and lyso-PE (Iwamoto et al., 2007). Fig. 1T indicates that biotinylated duramycin bound both convex and concave faces in symmetric liposomes. In contrast, only the concave face was labelled in asymmetric liposomes (Fig. 1U). Although we cannot distinguish which face is the outer and which the inner leaflet of the lipid bilayer in liposome specimen, these results indicate that our sample preparation protocol does not induce transbilayer redistribution of lipids during treatment.

Journal of Cell Science (2015) 128, 1627–1638 doi:10.1242/jcs.163105

Transbilayer distribution of phospholipids in membranes of human RBCs

The anti-PC antibody has been employed to study the membrane distribution of PC in various cells, including human RBCs, by using the SDS-FRL method (Fujimoto et al., 1996). The experiment has led to the observation that PC is distributed exclusively to the exoplasmic leaflet of RBCs. Consistent with these findings, our present results show that the gold particles were almost exclusively distributed to the exoplasmic fracture face (E-face) (Fig. 2A,B). A background level of gold particles was detected in the protoplasmic fracture face (P-face) (Fig. 2C,D). The average number of gold particles per μm^2 was 73.7±37.1 (n=19, mean±s.d.) in the E-face and 1.4±1.3 (n=19) in the P-face. It was calculated that 98.1% of PC was distributed in the outer leaflet of RBC membranes (Fig. 2Y). These results are similar to previous findings (Fujimoto et al., 1996).

In RBCs, SM clusters detected by MBP–lysenin were found primarily in the E-face (Fig. 2E,F), whereas a very low quantity of gold particles was detected in the P-face (Fig. 2G,H). The number of gold particles per μm^2 was 162.8±63.7 (n=22, mean±s.d.) in the outer leaflet and 2.5±1.4 (n=21) in the inner leaflet.

Previously, we have shown that the binding of lysenin to SM was inhibited by the presence of glycolipids (Ishitsuka et al., 2004; Makino et al., 2015). To examine the possibility that the low signal of MBP–lysenin in the inner leaflet was due to the high concentration of glycolipids, we studied the distribution of the main glycosphingolipid of RBCs, GM3 (Larson and Samuelsson,

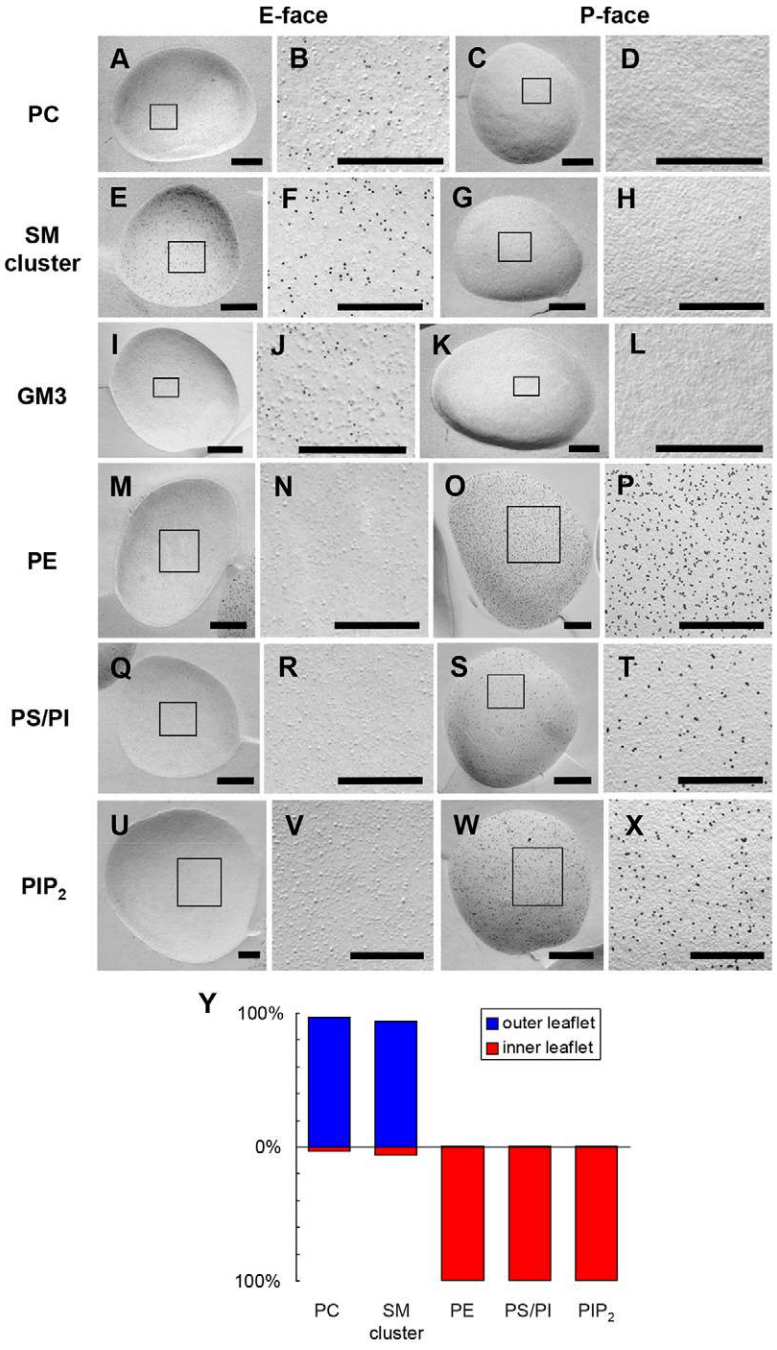

Fig. 2. Binding of the lipid probes to human RBC membranes. (A–D) Binding of anti-PC antibody. (A) E-face, (B) enlargement of the boxed area in A, (C) P-face, and (D) enlargement of the boxed area in C. (E–H) Binding of MBP–lysenin. (E) E-face, (F) enlargement of the boxed area in E, (G) P-face, (H) enlargement of the boxed area in G. (I–L) Binding of anti-GM3 antibody. (I) E-face, (J) enlargement of the boxed area in I, (K) P-face, (L) enlargement of the boxed area in K. (M–P) Binding of biotinylated duramycin. (M) E-face, (N) enlargement of the boxed area in M, (O) P-face, (P) enlargement of the boxed area in O. (Q–T) Binding of anti-PS/PI antibody. (Q) E-face, (R) enlargement of the boxed area in Q, (S) P-face, (T) enlargement of the boxed area in S. (U–X) Binding of anti-PIP_2 antibody. (U) E-face, (V) enlargement of the boxed area in U, (W) P-face, (X) enlargement of the boxed area in W. Scale bars: 500 nm. (Y) Transbilayer lipid distribution in RBC membrane. Average density of gold particles was compared in the outer and inner leaflets.

Journal of Cell Science

1980). Anti-GM3 antibody (Kotani et al., 1992) has been employed previously to visualise GM3 in mouse fibroblasts using SDS-FRL (Fujita et al., 2009a; Fujita et al., 2007), and supplementary material Fig. S3 shows SDS-FRL labelling of liposomes composed of GM3:PC (1:99) (A) and GM3:PE:PS (1:49.5:49.5) (B). Supplementary material Fig. S3 indicates that the anti-GM3 antibody bound the antigen highly efficiently in the liposomes that mimic the phospholipid composition of inner leaflet of the plasma membrane bilayer. Supplementary material Fig. S3C indicates that the antibody did not bind PE:PS liposomes in the absence of GM3.

In contrast to the model membrane results, the number of gold particles per μm^2 was 69.8±44.6 (n=19, mean±s.d.) in the outer leaflet (Fig. 2I,J), whereas it was 4.3±2.7 (n=19) in the inner leaflet (Fig. 2K,L) of RBCs. These results indicate that GM3 is enriched in the outer leaflet of RBCs and suggest that the low signal of MBP–lysenin in the inner leaflet was, indeed, due to the low concentration of SM clusters. Our results also indicate that 98.5% of SM clusters were distributed to the outer leaflet of the RBC membrane (Fig. 2Y).

In contrast to PC and SM clusters, PE was detected exclusively in the P-face by duramycin labelling (Fig. 2M-P). The number of gold particles per μm^2 was 0.6±0.7 (n=20, mean±s.d.) in the outer leaflet (E-face), whereas it was 177.5±47.7 (n=29) in the inner leaflet (P-face). This result suggests that 99.8% of PE was distributed to the inner leaflet of RBC membranes (Fig. 2Y). Previously, we have shown that the PE labelling by duramycin is dependent on the curvature of the membrane when the membrane is solid (Iwamoto et al., 2007). Duramycin did not efficiently bind low-curvature membranes, such as large liposomes composed of solid lipids (distearoyl-PE/distearoyl-PC). In contrast, duramycin is able to interact with low curvature membrane-containing PE when the lipids are fluid. It is speculated that the exposure of the hydrophobic moiety of the PE molecule is required for the binding of duramycin to PE. Although the RBC membrane has a comparatively lesser curvature than liposomes, duramycin yielded a positive signal in the specimen. In the SDS-FRL method, lipids are physically fixed by the deposition of platinum and carbon (Fujimoto et al., 1996; Fujita and Fujimoto, 2007). Our results suggest that, even after physical fixation, PE within membrane of RBCs is flexible enough to expose its hydrophobic region to duramycin.

Similar to staining of PE, PS/PI detection after incubation with anti-PS antibody (clone 1H6) was observed in the P-face, but was almost absent from the E-face (Fig. 2Q-T). The number of gold particles per μm^2 was 0.3±0.4 (n=22, mean±s.d.) in the outer leaflet but 43.9±27.5 (n=21) in the inner leaflet, suggesting that 99.3% of PS/PI are distributed in the inner leaflet of RBC membranes (Fig. 2Y).

Following staining of RBC membrane with the anti-PIP_2 antibody, immunogold particles were exclusively distributed to the P-face (Fig. 2U-X). The number of gold particles per μm^2 was 0.3±0.5 (n=21, mean±s.d.) in the outer leaflet, whereas it was 106.2±40.0 (n=24) in the inner leaflet, suggesting that 99.7% of PIP_2 are distributed in the inner leaflet of RBC membranes (Fig. 2Y).

Transbilayer distribution of phospholipids in HSF plasma membrane

Compared to the RBC membranes, the plasma membrane of HSFs is complex and heterogeneous. Here, we examined the distribution of various phospholipids in the outer and inner leaflets of flat regions and caveolae of the plasma membrane. Caveolae were identified by their characteristic shape as described previously (Fujimoto et al., 2000).

Immunogold particles were detected in the E-face of flat regions after incubation of HSF plasma membrane with the anti-PC antibody (Fig. 3A). Very little immunogold labelling was detected in the E-face of caveolae (Fig. 3B). In contrast to RBC membranes and tissues (Fujimoto et al., 1996), a significant amount of immunogold labelling was also found in the P-face of HSF plasma membrane (Fig. 3C,D). Furthermore, clusters of three to five gold particles were frequently associated with caveolae (Fig. 3D arrowheads) in the P-face. The average number of gold particles per μm^2 was 7.1±3.6 (n=50, mean±s.d.) in the E-face, and 1.5±1.4 (n=39) in the P-face. This indicates that 82.6% of PC was distributed in the outer leaflet of HSF plasma membrane (Fig. 3R).

Compared to RBCs, the membrane density of PC was ten times lower in HSFs. We then examined membrane distribution of PC in HeLa cells. Supplementary material Fig. S4 indicates the distribution of immunogold particles in the flat region (supplementary material Fig. S4A,C) and caveolae (supplementary material Fig. S4B,D) of the plasma membrane of HeLa cells. The average number of gold particles per μm^2 was 40.2±28.2 (n=16, mean±s.d.) in the E-face, and 3.4±1.6 (n=19) in the P-face. It was calculated that 92.2% of PC was distributed in the outer leaflet of HeLa cell plasma membranes. We did not detect PC associated to caveolae in HeLa cells. Membrane density of PC in HeLa cells was comparable to that in RBCs. These results indicate that membrane density of PC is cell type specific.

Similar to PC, SM clusters revealed by MBP–lysenin binding were mainly distributed in the E-face (Fig. 3E) of the HSF plasma membrane. Signals were often observed at the edge and the centre of caveolae (Fig. 3F arrowheads). In contrast to RBCs, significant numbers of gold particles were detected in the P-face where they formed a domain of 5–20 particles (Fig. 3G). Inner leaflets of caveolae were devoid of gold particles (Fig. 3H). The number of gold particles per μm^2 was 24.9±12.4 (n=42, mean±s.d.) in the outer leaflet, whereas it was 3.4±3.8 (n=43) in the inner leaflet. These results suggest that 87.9% of SM clusters detected by MBP–lysenin were distributed in the outer leaflet of the fibroblast plasma membrane (Fig. 3R).

In contrast to PC and SM distribution, PE labelling by duramycin was demonstrated almost exclusively in the P-face (Fig. 3I-K). Signals were often observed within the rim of caveolae (Fig. 3K arrowheads). The average number of gold particles per μm^2 was 1.1±0.7 (n=38, mean±s.d.) in the outer leaflet (E-face), whereas it was 45.8±16.6 (n=34) in the inner leaflet (P-face). This result suggests that 97.7% of PE distributes in the inner leaflet of HSF plasma membrane (Fig. 3R).

Similar to PE staining, localisation of the acidic phospholipids PS and PI was indicated almost exclusively in the P-face, whereas only a few gold particles stained the E-face (Fig. 3L-N). Signals were often associated with the edge of caveolae (arrowheads) in the P-face (Fig. 3N). The number of gold particles per μm^2 was 0.5±0.3 (n=40, mean±s.d.) in the outer leaflet, whereas it was 11.8±4.2 (n=32) in the inner leaflet, suggesting that 95.8% of PS/PI were distributed in the inner leaflet of HSF plasma membranes (Fig. 3R).

Similar to the distribution of PIP_2 in the RBC membrane, immunogold particles were almost exclusively distributed in the P-face in HSF plasma membrane following incubation with the anti-PIP_2 antibody (Fig. 3O-Q). The gold particles often localised

Journal of Cell Science (2015) 128, 1627–1638 doi:10.1242/jcs.163105

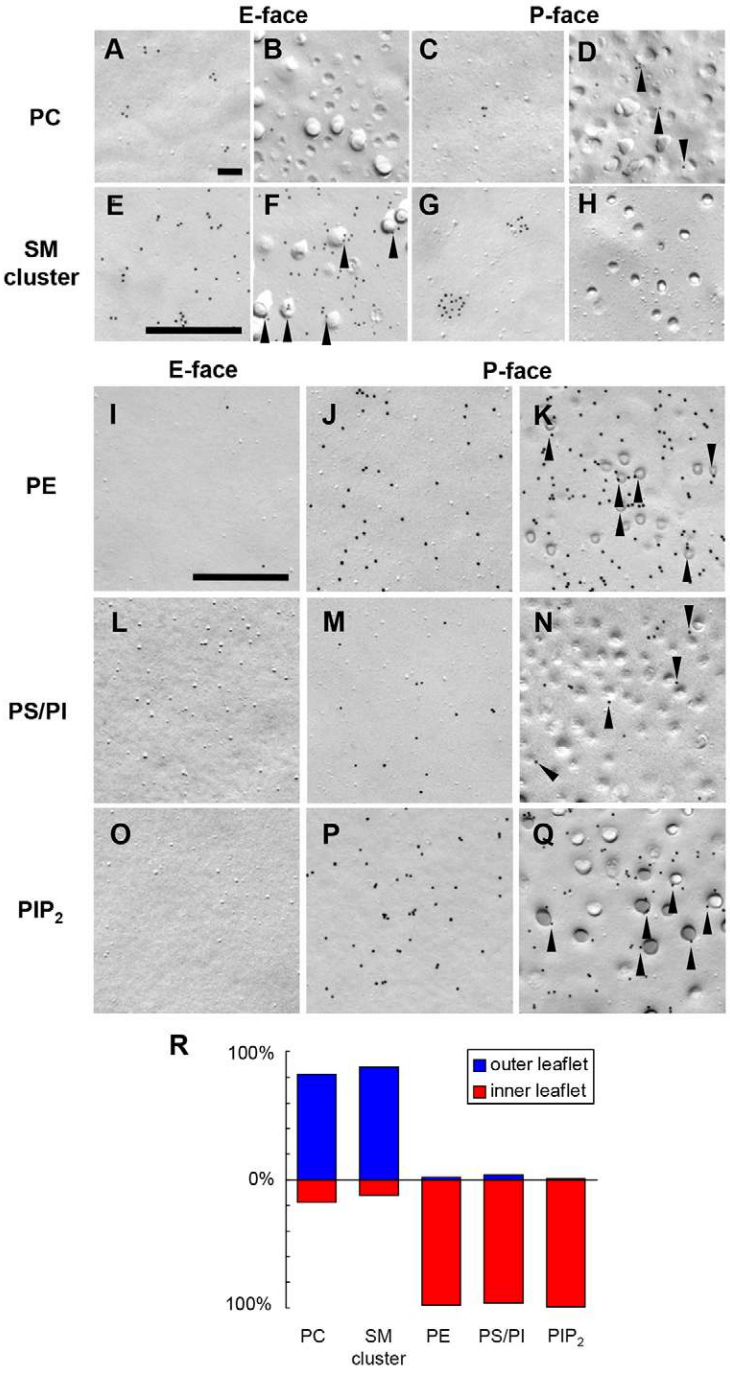

Fig. 3. Binding of the lipid probes to HSF plasma membranes. (A–D) Binding of anti-PC antibody. (A) E-face in flat region, (B) E-face in caveolae, (C) P-face in flat region, and (D) P-face in caveolae. Small immunogold aggregates associated with caveolae (arrowheads). (E–H) Binding of MBP–lysenin. (E) E-face in flat region, (F) E-face in caveolae. Some signals were detected in the center of and at the rim of caveolae (arrowheads). (G) P-face in flat region. Gold assemblies indicating the lipid domains enriched with SM clusters in P-face. (H) P-face in caveolae. (I–K) Binding of biotinylated duramycin. (I) E-face, (J) P-face in flat region, (K) P-face in caveolae. Several gold particles showing the distribution of PE at the rim of caveolae (arrowheads). (L–N) Binding of anti-PS/PI antibody. (L) E-face, (M) P-face in flat region, (N) P-face in caveolae. (O–Q) Binding of anti-PIP_2 antibody. (O) E-face, (P) P-face in flat region, (Q) P-face in caveolae. Many caveolae were immunogold-labelled at the rim (arrowheads). Scale bar in A for A–D, 100 nm; in E for E–H, 500 nm; in I for I–Q, 500 nm. (R) Transbilayer lipid distribution in HSF plasma membrane. Average density of gold particles was compared in the outer and inner leaflets.

in the periphery of caveolae (Fig. 3Q, arrowheads), consistent with the previous reports (Fujita et al., 2009b). The number of gold particles per μm^2 was 0.3±0.2 (n=41, mean±s.d.) in the outer leaflet, whereas it was 39.1±13.2 (n=35) in the inner leaflet, suggesting that 99.2% of PIP_2 are distributed in the inner leaflet of fibroblast plasma membranes (Fig. 3R).

Lateral distribution of phospholipids in the plasma membrane

We then analysed the lateral distribution of gold particles in RBC and HSF plasma membranes in a statistical analysis using Ripley's K-function (Haase, 1995; Kiskowski et al., 2009; Ripley, 1979). This method has been applied to analyse the distribution of SM clusters (Abe et al., 2012; Kiyokawa et al., 2005), gangliosides (Fujita et al., 2007; Kiyokawa et al., 2005), PIP_2 (Abe et al., 2012; Fujita et al., 2009b), glycophospholipid (Murate et al., 2010), cholesterol (Mizuno et al., 2011) and proteins (Lillemeier et al., 2006; Prior et al., 2003; Wilson et al., 2004) in the plasma membrane.

The estimated radius of clusters, number of detected clusters and maximum value of L(r)-r in each analysis are shown in Table 1 for RBCs, and Table 2 for HSFs. Table 1 indicates that PC and GM3 formed domains in the outer leaflet of the RBCs in more than half of specimens tested. Regarding SM clusters in the outer leaflet, only one out of 22 analyses exhibited domains, whereas 21 analyses indicated a random distribution. In the inner

leaflet of RBCs, PS/PI and PIP_2 exhibited domains in more than half of specimens. Three out of 29 analyses showed domains of PE in the inner leaflets, whereas the remaining 26 indicated a random distribution.

In the HSF plasma membrane (Table 2), outer-leaflet PC and SM clusters, as well as inner-leaflet PS/PI and PIP_2 exhibited immunogold-labelled domains in all samples. In the case of SM clusters, 28 out of 43 areas exhibited immunogold-labelled domains also in the inner leaflet, whereas 15 areas showed a random distribution of immunogold-labelled domains. Twenty out of 34 analyses exhibited domains of PE in the inner leaflet, whereas the remaining 14 displayed a random distribution.

Transbilayer distribution of SM clusters in human neutrophil plasma membrane

SM clusters were not observed in the inner leaflet of RBCs (Fig. 2E-H), but formed clear domains in the inner leaflet of HSF plasma membranes (Fig. 3G and Table 2). We examined whether other cell types show such lipid domains in the inner leaflet of the plasma membrane. Fig. 4A,B show the distribution of SM clusters revealed by MBP–lysenin in the E- (Fig. 4A) and P-faces (Fig. 4B) of neutrophil plasma membranes. As shown in HSF plasma membranes, SM clusters in neutrophil plasma membranes were mainly distributed in the E-face and, also similar to HSFs, clear domains were observed in the P-face. Because of the rough surface of neutrophil plasma membranes, it was difficult to accurately quantify the density of immunogold particles within a large area. However, the domain radii were estimated to be 110.1±50.0 nm (n=8, mean±s.d.) in the inner leaflet of neutrophils. The size of domains was not statistically different to those in HSFs (Table 2); calculated using by Mann–Whitney U test (P=0.18).

Scrambled transbilayer distribution of phospholipids in the microparticles derived from thrombin-stimulated platelets

Similar to the situation in RBCs, the asymmetric distribution of phospholipids in the plasma membrane of resting platelets has been reported (Perret et al., 1979; Schick et al., 1976). However, estimating the transbilayer distribution of the lipids is technically difficult in a conventional phospholipase procedure due to the presence of intracellular membranes. Activation of platelets is accompanied by the release of highly procoagulant (Sinauridze et al., 2007) and annexin-V-positive microparticles (Thiagarajan and Tait, 1991). Binding of annexin V suggests the exposure of PS in microparticle membranes. However, annexin V also binds to PA, PI and PE (Blackwood and Ernst, 1990; Schlaepfer et al., 1987). The detailed distribution of lipids in microparticle membrane has not been examined. In our present study, we examined the transbilayer and lateral distribution of SM clusters, and PS/PI in resting and thrombin-stimulated platelets as well as platelet microparticles.

In non-stimulated platelet plasma membrane, PS/PI labelling was almost absent from the E-face (Fig. 5A,B), but observed in the P-face (Fig. 5C,D). These results are similar to those observed in RBC membrane (Fig. 2Q-T) and HSF plasma membrane (Fig. 3L-N). In contrast to PS/PI, the localisation of SM clusters revealed by MBP–lysenin was exclusively detected in the E-face (Fig. 5E,F) of platelet plasma membrane. Only a background level of gold particles was observed in the P-face (Fig. 5G,H). The exclusive distribution of SM clusters in the E-face of platelet plasma membranes is similar to that in RBC membranes, but different to nucleated HSFs and neutrophils.

Treatment of platelet-rich plasma with 0.5 units/ml thrombin for 3 min did not significantly alter the transbilayer distribution of PS/PI (Fig. 5I-L) and SM clusters (Fig. 5M-P). In contrast, significant numbers of gold particles that correspond with the localisation of PS/PI were detected both in the E- (Fig. 5Q) and P-faces (Fig. 5R) of microparticle membranes derived from activated platelets. Anti-PS/PI antibody labelling was detected in the E-face in 44.3% (n=79) of microparticles. The distribution of MBP–lysenin staining was also observed in both layers of microparticle membrane (Fig. 5S,T). Notably, signals for PS/PI as well as SM clusters were not evenly distributed in outer and inner leaflets (Fig. 5Q-T) of microparticles.

In a limited number of activated platelets, PS/PI was detected within a very restricted area of the outer leaflet (Fig. 6A,B). Fig. 6C,D indicates that the E-face of budding microparticles shows a PS/PI signal, whereas other parts of E-face of the membrane were not labelled by the anti-PS/PI antibody. These results suggest that the scrambled membrane domains are released as microparticles once the platelets are activated by thrombin.

DISCUSSION

In our study here, we employed the SDS-FRL method together with a variety of lipid-binding proteins and a peptide to study the transbilayer and lateral distribution of phospholipids in RBC membranes as well as plasma membranes from HSFs, HeLa cells, neutrophils and platelets. Our results indicated that the distribution of phospholipids in RBC membranes was discrete; PC and SM clusters were exclusively localised in the outer leaflet, whereas PE, PS/PI and PIP_2 were restricted in the inner leaflet. These results are in contrast to previous biochemical characterisations, in which each phospholipid was detected in

Table 1. Lipid domain analyses of phospholipids for the RBC membrane

	Outer leaflet				Inner leaflet			
	Radius (nm) (mean±s.d.)	Lipid domain	Maximum value (mean±s.d.)	Actual domain radius(nm)	Radius (nm) (mean±s.d.)	Lipid domain	Maximum value (mean±s.d.)	Actual domain radius (nm)
PC	24.6±8.8	10/19	7.8±5.8	random	–	0/19	–	–
SM cluster	random	1/22	1.8±8.2	random	–	0/21	–	–
GM3	32.8±5.5	12/19	16.7±11.2	2–15	–	0/19	–	–
PE	–	0/20	–	–	random	3/29	0.5±1.8	random
PS/PI	–	0/22	–	–	16.5±1.6	19/21	26.2±20.1	random
PIP_2	–	0/22	–	–	16.5±0.5	14/24	8.2±4.8	random

–: Insufficient number of gold particles for analysis.

Journal of Cell Science (2015) 128, 1627–1638 doi:10.1242/jcs.163105

Table 2. Lipid domain analyses of phospholipids for the HSF plasma membrane

	Outer leaflet				Inner leaflet			
	Radius (nm) (mean±s.d.)	Lipid domain	Maximum value (mean±s.d.)	Actual domain radius (nm)	Radius (nm) (mean±s.d.)	Lipid domain	Maximum value (mean±s.d.)	Actual domain radius (nm)
PC	39.6±14.9	50/50	123.6±66.6	1–30	–	0/39	–	–
SM cluster	36.1±7.9	42/42	30.5±22.6	3–20	147.7±60.6	28/43	646.5±220.2	60–180
PE	–	0/38	–	–	20.7±2.0	20/34	6.7±4.5	random
PS/PI	–	0/40	–	–	22.8±7.0	32/32	49.2±26.6	1–20 in some samples
PIP_2	–	0/41	–	–	19.6±3.3	35/35	18.0±11.6	random

–: Insufficient number of gold particles for analysis.

both leaflets, although the distribution was asymmetric (Bretscher, 1972a; Bretscher, 1972b; Bütikofer et al., 1990; Devaux, 1991; Gordesky et al., 1972; van Meer et al., 1981; Verkleij et al., 1973; Zachowski, 1993). Since our method is dependent on the lipid probes employed, it is possible that lipid concentration was not sufficiently high to be detected by the probes. However, the model membrane experiments demonstrated that our probes effectively detected the lipids, even when the membrane concentration was as low as 1% (mol/mol). We speculate that the discrepancy between our results and previously published biochemical studies is due to leakage and re-organisation of lipid molecules occurring during biochemical analyses.

To evaluate the size of phospholipid domains when using the SDS-FRL method, the distance between target molecule and gold particle has to be calculated. When 2 nm gold-conjugated glutathione *S*-transferase (GST) was labelled with anti-GST antibody followed by a 5 nm gold-conjugated $F(ab')_2$ fragment of the secondary antibody, the distance between the surface of 2 nm gold and the centre of 5 nm gold was measured to be 16 nm (Fujita et al., 2007). To label SM clusters, we added MBP–lysenin, anti-MBP antibody and 10 nm gold-conjugated secondary IgG antibody. In this labelling protocol, the distance between SM cluster and gold was estimated to be 25 nm. The distance between the lipid and gold particle was shorter when the two-step labelling protocol to reveal PC, GM3, PE, PS/PI and PIP_2 was employed. Considering the distance between the lipid and the gold particle, we estimated the distribution of phospholipids as follows: random (PC and SM cluster at the outer leaflet of RBC membranes, PE and PIP_2 in the inner leaflets of RBC and HSF plasma membrane and PS/PI in the inner leaflets of RBC), domains with a radius of 2–15 nm (GM3 in the outer leaflet of RBC membrane), domains with a radius of 1–30 nm (PC in the outer leaflet of HSF plasma membrane), domains with a radius of 3–20 nm (SM cluster in the outer leaflet of HSF plasma membrane) and domains with a radius of 60–180 nm (SM cluster in the inner leaflet of HSF plasma membrane) (see Table 1 for RBCs and Table 2 for HSFs). In case of PS/PI domains in HSF plasma membrane, there was a big deviation in the domain radii (13.9–44.9 nm, average 22.8 nm); and nine out of 32 analyses indicated domains with a radius bigger than 25 nm. These results suggest the existence of small number of PS/PI domains in the plasma membrane. Our finding that the SM cluster is randomly distributed in RBC membranes indicates that multivalent binding of gold-conjugated secondary antibodies did not induce artificial aggregation of immunogold clusters.

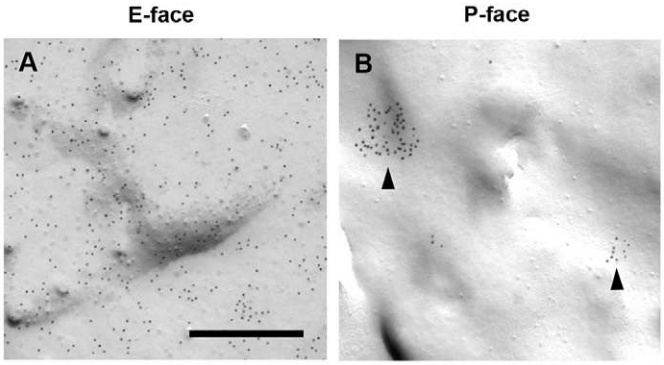

Fig. 4. Binding of MBP–lysenin to human neutrophil plasma membranes. (A) E-face, (B) P-face. Gold particles indicate that the accumulation of SM clusters formed distinctive domains at the P-face (arrowheads). Scale bar: 500 nm.

Our results revealed that the lateral distribution of not only SM clusters, but also of PC was not random in the outer leaflet of HSF plasma membranes. In addition, PS/PI occasionally formed domains in the inner leaflet. In case of RBC membranes, GM3 formed domains in the outer leaflet. Lipid domains composed of sphingolipids and cholesterol attracts considerable attention (Jacobson et al., 2007; Lingwood and Simons, 2010). It has already been reported that many kinds of membrane lipid, including SM (Abe et al., 2012; Kiyokawa et al., 2005), glycosphingolipid (Fujita et al., 2007; Iwabuchi et al., 2008; Kiyokawa et al., 2005), glycosphingolipid (Murate et al., 2010) and cholesterol (Mizuno et al., 2011) form domains on the plasma membrane. Recently, we clarified the physiological transbilayer cooperation between SM and PIP_2 domains across the plasma membrane during cytokinesis, by using superresolution fluorescence microscopy (Abe et al., 2012). Our present results, obtained by using the SDR-FRL method, will contribute to better understand the role of specific lipid domains in each leaflet of the plasma membrane.

In contrast to RBC plasma membranes, PC and SM clusters formed distinct lipid domains in the inner leaflet of HSF plasma membranes (as seen by labelling with 3–20 gold particles). Domains of SM clusters were also observed in the inner leaflet of the neutrophil plasma membranes with comparable radii. It has been reported that PC in the cytoplasmic side of the plasma membrane is hydrolysed by PC-specific phospholipase C (Ramoni et al., 2004) and phospholipase D2 (PLD2) (Du et al., 2004). Sphingomyelin is also digested by intracellular neutral sphingomyelinase 2 (Tani and Hannun, 2007). In both cases, signalling lipids, including diacylglycerol, PA, ceramide and sphingosine-1-phosphate (Nagata et al., 2006) are formed. Our results suggest that the inner-leaflet lipid domains of PC and SM may be the targets of these enzymes in fibroblast and neutrophil

Journal of Cell Science (2015) 128, 1627–1638 doi:10.1242/jcs.163105

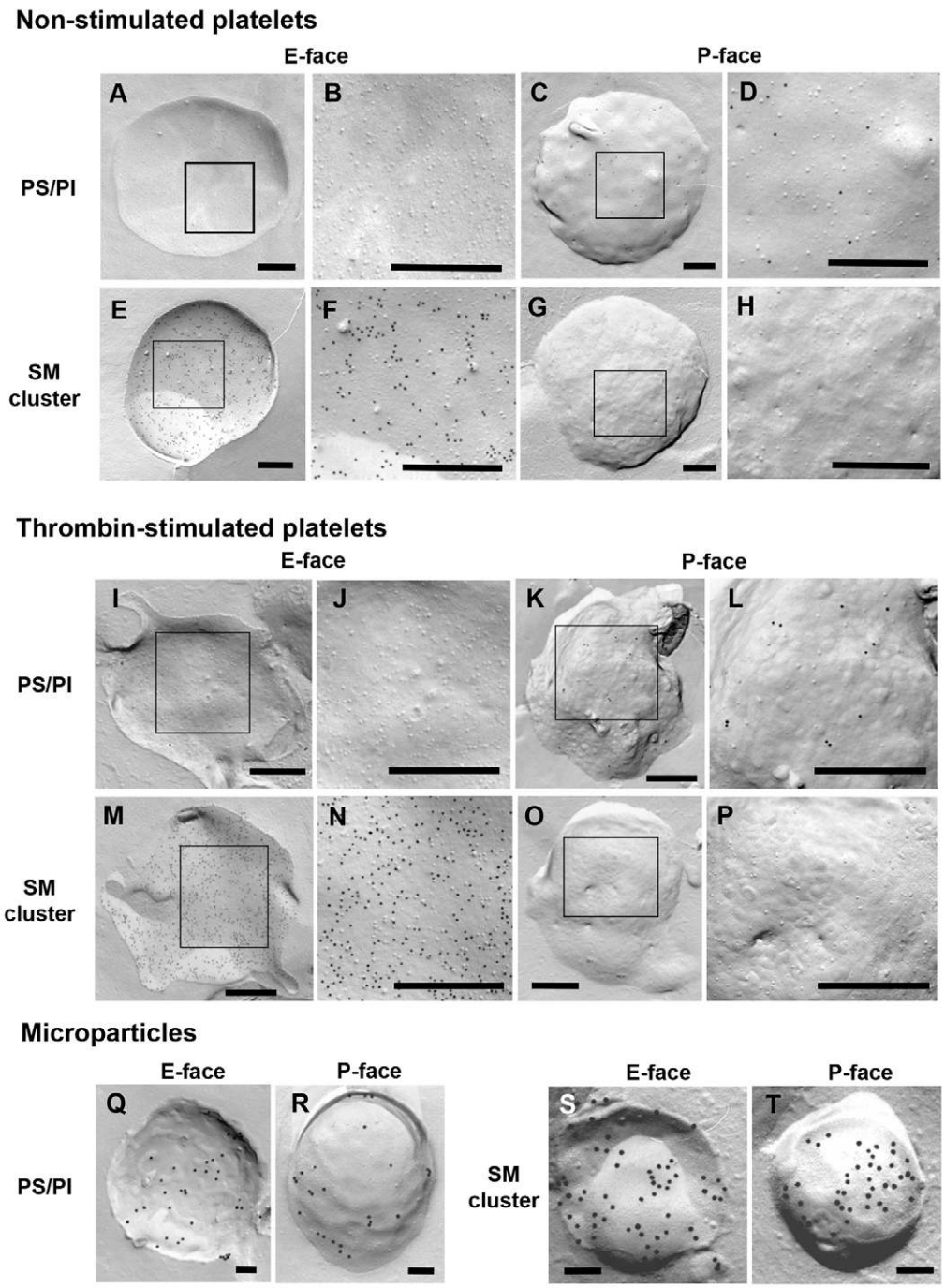

Fig. 5. Binding of the lipid probes to non-stimulated and thrombin-stimulated human platelet plasma membranes and microparticle membranes. (A–D) Binding of anti-PS/PI antibody to non-stimulated platelet plasma membrane. (A) E-face, (B) enlargement of the boxed area in A, (C) P-face, (D) enlargement of the boxed area in C. (E–H) Binding of the SM-cluster-specific probe, MBP–lysenin to non-stimulated platelet plasma membrane. (E) E-face, (F) enlargement of the boxed area in E, (G) P-face, (H) enlargement of the boxed area in G. (I–L) Binding of anti-PS/PI antibody to thrombin-stimulated platelet plasma membrane. (I) E-face, (J) enlargement of the boxed area in I, (K) P-face, (L) enlargement of the boxed area in K. (M–P) Binding of MBP–lysenin to thrombin-stimulated platelet plasma membrane. (M) E-face, (N) enlargement of the boxed area in M, (O) P-face, (P) enlargement of the boxed area in O. (Q,R) Binding of anti-PS/PI antibody to E- (Q) and P-face (R) of microparticle membrane. (S,T) Binding of MBP–lysenin to E-face (S) and P-face (T) of microparticle membrane. Scale bars: 500 nm (A–P), 100 nm (Q–T).

plasma membranes. In contrast to the present study, intracellularly expressed lysenin did not localise to the plasma membrane in living cells (Abe et al., 2012). Successful detection of SM domains in the inner leaflet in the present study may be due to the washing out of SM-associated proteins following SDS treatment. The molecular mechanism of the distribution of SM in the inner leaflet of the plasma membranes from HSF and neutrophils is obscure. However, recent results using equinatoxin–EGFP as a SM probe suggest the exposure of SM to the cytoplasmic side of *cis*-Golgi compartment in fibroblasts (Bakrac et al., 2010). These results suggest that the exposure of SM to the inner leaflet of the plasma membranes in HSF is dependent on the active *de novo* biosynthesis of SM, which is defective in RBC.

Caveolae are characteristic small pits (60–80 nm in diameter) of the plasma membrane that play important roles in cellular signalling, endocytosis, lipid metabolism as well as mechanosensing (Bastiani and Parton, 2010). Although the enrichment of sphingomyelin in caveolae has been biochemically demonstrated (Ortegren et al., 2004), previous SDS-FRL detection of SM using monoclonal antibody, that binds both SM and saturated fatty acid-containing PC (Hirota et al., 1995), did not indicate the enrichment of SM in caveolae (Fujimoto, 1996). Our results showed the occasional appearance of SM cluster in the centre and the edge of the outer leaflet of caveolae. Although SM clusters were observed in the inner leaflet of the plasma membranes of HSF, the inner leaflet of caveolae was devoid of SM clusters, suggesting that outer-leaflet

Journal of Cell Science (2015) 128, 1627–1638 doi:10.1242/jcs.163105

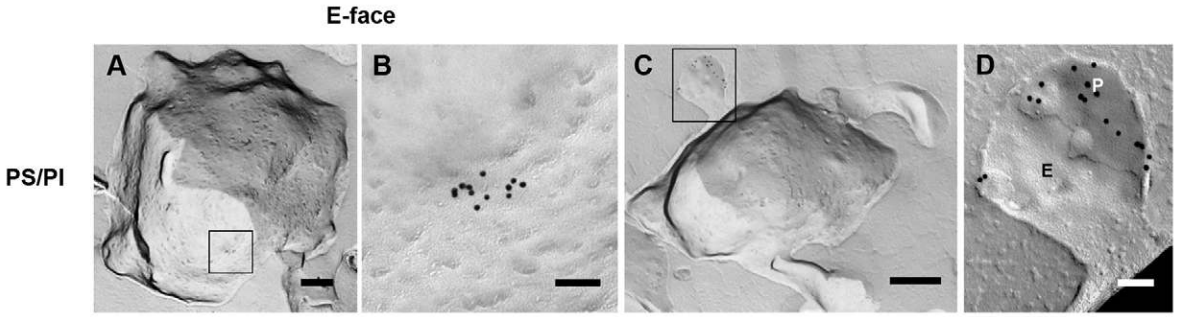

Fig. 6. Binding of anti-PS/PI antibody to thrombin-stimulated platelet plasma membranes. (A) E-face, (B) enlargement of the boxed area in A, (C) freeze-fracture image of budding microparticle, (D) enlargement of the boxed area in C. E, E-face; P, P-face. Scale bars: 500 nm (A,C), 100 nm (B,D).

SM and inner-leaflet SM localise independently in caveolae. In contrast, we detected PC in the rim of the inner leaflet of caveolae in HSF. The outer leaflet of caveolae was devoid of PC. These results suggest that PC in the outer and inner leaflet do not coordinate across the bilayer in caveolae. Recently it has been reported that type IV P-type ATPase ATP8B1/ATP8B2 preferentially translocates PC from the outer to the inner leaflet of the plasma membrane (Takatsu et al., 2014). Our results suggest that caveolae are the site of the transbilayer movement of PC in HSFs.

PIP_2 was also frequently detected in the rim of caveolae in the inner leaflet. Similar to PIP_2, PE in the inner leaflet was localised within the rim of caveolae. Although the depth of caveolae were different in the specimen, labelling of the rim of caveolae was observed regardless of caveolar depth, suggesting that it is not simply caused by superimposition of gold particles along the lateral wall of the deeply invaginated caveolae. Similar results have been obtained by Fujita et al. (Fujita et al., 2009b). Because of its small headgroup, PE has tendency to form corn-shape (Cullis and de Kruijff, 1979). This structural feature of the lipid may be involved in the formation of high curvature in the edge of caveolae.

Similar to the RBC membrane, SM clusters and PS/PI were exclusively distributed in the outer and inner leaflet, respectively, within the platelet plasma membrane. Even after thrombin activation, platelets showed clear asymmetry of SM clusters and PS/PI. However, some cells showed positive signals of PS/PI in the restricted area of the outer leaflet of the plasma membrane. We also observed selective labelling of the outer leaflet of budding membrane with the anti-PS/PI antibody. The released microparticle fraction showed scrambled transbilayer lipid distribution of SM clusters and PS/PI. These results indicate that the scrambled membranes are selectively released in the form of microparticles in thrombin-activated platelets and also suggest that exposure of PS/PI to the outer leaflet triggers the vesiculation of platelets.

Our results, as well those from as others (Cheng et al., 2014; Fujimoto et al., 1996; Fujita et al., 2007; Fujita et al., 2009b; Murate et al., 2010), indicate that the SDS-FRL method is a useful and powerful technique for investigating the localisation of membrane lipids. It has the following advantages: (1) the extremely rapid freezing procedure (milliseconds) and chemical fixative-free methods ensures minimal re-organisation of the membrane lipids during sample preparation; (2) SDS digestion removes lipid-binding or lipid-associated proteins and most of the membrane lipids are exposed to lipid probes; (3) the localisation of lipids in the inner and the outer leaflets can be distinguished by physically splitting each leaflet of the lipid bilayer; (4) the two-dimensional distribution of the lipids can also be investigated at nanometre level and; (5) this method can be applied to any cell, tissue and organelle.

The successful detection of lipids by SDS-FRL primarily depends on the properties of the lipid probes. Owing to the lower antigenicity of lipids, only a few lipid-specific antibodies are available for staining. Furthermore, a limited number of peptides and proteins are reported to bind specific lipids (Hullin-Matsuda and Kobayashi, 2007). Further development and characterisation of lipid probes is important for the future application of SDS-FRL in lipid biology.

MATERIALS AND METHODS

Lipid membranes and liposomes

POPC, egg SM, DOPE, POPE, lyso-PE, POPS, 1-palmitoyl-2-oleoyl-*sn*-glycero-3-phosphate (POPA), L-α-phosphatidylinositol from bovine liver (liver PI) and L-α-phosphatidylinositol (4,5)-bisphosphate from porcine brain (brain PIP_2) were purchased from Avanti Polar Lipids (Alabaster, AL). GM3 was from Matreya, LLC (Pleasant Gap, PA). Cholesterol was from Sigma-Aldrich (St Louis, MO). The lipids were mixed at defined molar ratios and dried under vacuum overnight. The samples were dissolved slowly into Tris-buffered saline pH 7.4 (TBS) with three cycles of heating and cooling, sonicated in a bath sonicator for 10 min to prepare multilamellar vesicles (MLVs). MLVs were centrifuged (21,600 ***g***) for 10 min at 4℃ and the precipitate was re-suspended in TBS containing 1.75 M sucrose to prevent the formation of ice crystals. The specimens were sandwiched between two replica carriers (Bal-Tec, Liechtenstein) and rapidly frozen in liquid ethane cooled by liquid nitrogen. To prepare asymmetric liposomes, MLVs composed of POPC:cholesterol (1:1) in TBS were freeze-thawed three times using liquid nitrogen and a 37℃ water bath, and then extruded 20 times through polycarbonate membranes (0.4 µm, Avanti) mounted in the Mini-Extruder (Avanti). Ten % (mol/mol) lyso-PE was then added to the liposomes. Control symmetric liposomes were prepared by freeze-thawing and extruding MLVs composed of lyso-PE:POPC:cholesterol (10:45:45). Both symmetric and asymmetric liposomes were centrifuged, re-suspended, sandwiched and quickly frozen as described above.

Human red blood cells, skin fibroblasts, HeLa cells, neutrophils and platelets

Erythrocytes were obtained from freshly drawn human blood. The cells were washed with phosphate-buffered saline three times, sandwiched between two carriers (Bal-Tec). Human skin fibroblasts were grown on coverslips in Ham's F-10 Nutrient Mixture (Gibco, Grand Island, NY) containing 10% fetal bovine serum (FBS) and penicillin/streptomycin. HeLa cells were grown in Dulbecco's Modified Eagle's Medium (Gibco) containing 10% FBS and penicillin/streptomycin. These cultured cells

were covered with copper plates. Human neutrophils were prepared as previously reported (Iwabuchi et al., 2008). The isolated cells from freshly drawn blood were sandwiched between two carriers. Platelets were prepared from freshly drawn blood as previously reported (Kasahara et al., 2013). The platelet-rich plasma was activated with 0.5 units/ml thrombin (Sigma-Aldrich) for 3 min at 37℃. Activated and control platelets were fixed with a final concentration of 2% paraformaldehyde, washed with Tyrode's buffer (137 mM NaCl, 2.7 mM KCl, 3.75 mM NaH_2PO_4, 5 mM HEPES pH 7.4, 0.35% BSA and 5 mM glucose), sandwiched between two carriers. All cells were quickly frozen by liquid ethane cooled by liquid nitrogen. This research using human blood was followed the Ethical Regulations for Research Involving Human Subjects in RIKEN.

SDS-FRL method

Frozen samples were fractured at −110℃ and replicated by an evaporation of carbon–platinum–carbon in a freeze-etch unit (BAF400T, Balzers). Replicated samples were digested in 2.5% SDS and 10% glycerol in 62.5 mM Tris buffer (pH 6.8) in the absence or presence of 5% β-mercaptoethanol for more than 12 h at room temperature or 60℃ under vigorous stirring (Murate et al., 2010). The replicas were thoroughly washed with TBS, and treated with 2% BSA and 0.2% gelatin to prevent non-specific binding of probes. PC was labelled with anti-PC monoclonal antibody (Nam et al., 1990), SM was detected with MBP–lysenin (Kiyokawa et al., 2005), and GM3 was labelled with mouse anti-GM3 antibody (Seikagaku Corp., Japan) (Kotani et al., 1992). PE and lyso-PE were detected with biotinylated duramycin (Iwamoto et al., 2007), PS with His-Lact-C2 (Yeung et al., 2008), mouse anti-PS antibody (clone PS4A7) (Umeda et al., 1989), or mouse anti-PS monoclonal antibody (clone 1H6, Upstate, Lake Placid, NY), and PIP_2 with mouse anti-PIP_2 monoclonal antibody (Miyazawa et al., 1988). His–Lact-C2 was prepared as follows: pET28–EGFP–Lact-C2 expressing EGFP-Lact-C2 was constructed by replacing D4 on pET28–EGFP-D4 (Shimada et al., 2002) with polymerase chain reaction-amplified Lact-C2. Recombinant protein was expressed in *E. coli* strain BL21 (DE3) (Novagen, Madison,WI) and purified using HisTrap FF crude column (GE Healthcare, UK). After labelling, the replicas were washed with TBS and incubated with 10 nm gold-conjugated anti-mouse IgM (British BioCell International, UK) for PC, GM3 and PS (clone PS4A7), anti-mouse IgG (Amersham, UK) for PS/PI (clone 1H6) and PIP_2, or 15 nm gold-conjugated anti-biotin antibody (British BioCell International) for PE. For detection of SM, the replicas were incubated with rabbit anti-MBP antibody (New England BioLabs, MA), washed with TBS, and incubated with 10 nm gold-conjugated anti-rabbit IgG (Amersham). For detection of PS using His-Lact-C2, samples were incubated with mouse anti-Penta-His antibody (Qiagen, Germany), washed with TBS and incubated with 10 nm gold-conjugated anti-mouse IgG antibody (Amersham). After immunogold labelling, the replicas were washed with TBS, washed again with ultrapure water, and then picked onto pioloform-coated grids. Specimens were examined under transmission electron microscope (1200EX-II or JEM1230, JEOL, Japan) with the help of the Support Unit for Neuromorphological Analysis or the Materials Characterisation Team in RIKEN. Electron micrographs were recorded on imaging plates, scanned and digitised by an FDL 5000 imaging system (Fuji Photo Film, Japan) or taken by a charge-coupled device (CCD) camera (Veleta, Olympus-SIS, Germany).

Image analysis

Lateral distribution of gold particles on plasma membrane was analysed using L-function (Haase, 1995; Kiskowski et al., 2009; Ripley, 1979) as previously reported (Abe et al., 2012; Kiyokawa et al., 2005; Murate et al., 2010). Briefly, the *xy* coordinates of each gold particle were obtained with ImageJ public domain software, and analysed by L-function using SpPack software (Perry, 2004).

Acknowledgements

We thank George L. W. Perry for software used for the statistical analysis of gold particles. We are grateful to Peter Greimel, Françoise Hullin-Matsuda, Takehiko Inaba, Reiko Ishitsuka, Steven Jones, Takuma Kishimoto and Nario Tomishige for critical reading of the manuscript.

Competing interests

The authors declare no competing or financial interests.

Author contributions

T.K. conceived and coordinated the project. M.M. performed electron microscopy experiments and data analysis. M.A. and M.U generated probes. K.K. and K.I. prepared platelets and neutrophils. M.M. and T.K. wrote the manuscript.

Funding

This work was supported by The Naito Foundation, Lipid Dynamics Program and Integrated Lipidology Program of RIKEN, Grant-in-Aid for Scientific Research [grant number 23590251 to M.M.] and [grant numbers 22390018 and 24657143 to T.K.] from the Ministry of Education, Culture, Sports, Science and Technology of Japan.

Supplementary material

Supplementary material available online at
http://jcs.biologists.org/lookup/suppl/doi:10.1242/jcs.163105/-/DC1

References

Abe, M., Makino, A., Hullin-Matsuda, F., Kamijo, K., Ohno-Iwashita, Y., Hanada, K., Mizuno, H., Miyawaki, A. and Kobayashi, T. (2012). A role for sphingomyelin-rich lipid domains in the accumulation of phosphatidylinositol-4,5-bisphosphate to the cleavage furrow during cytokinesis. *Mol. Cell. Biol.* **32**, 1396-1407.

Bakrac, B., Kladnik, A., Macek, P., McHaffie, G., Werner, A., Lakey, J. H. and Anderluh, G. (2010). A toxin-based probe reveals cytoplasmic exposure of Golgi sphingomyelin. *J. Biol. Chem.* **285**, 22186-22195.

Bastiani, M. and Parton, R. G. (2010). Caveolae at a glance. *J. Cell Sci.* **123**, 3831-3836.

Blackwood, R. A. and Ernst, J. D. (1990). Characterization of Ca2(+)-dependent phospholipid binding, vesicle aggregation and membrane fusion by annexins. *Biochem. J.* **266**, 195-200.

Bretscher, M. S. (1972a). Asymmetrical lipid bilayer structure for biological membranes. *Nat. New Biol.* **236**, 11-12.

Bretscher, M. S. (1972b). Phosphatidyl-ethanolamine: differential labelling in intact cells and cell ghosts of human erythrocytes by a membrane-impermeable reagent. *J. Mol. Biol.* **71**, 523-528.

Bütikofer, P., Lin, Z. W., Chiu, D. T., Lubin, B. and Kuypers, F. A. (1990). Transbilayer distribution and mobility of phosphatidylinositol in human red blood cells. *J. Biol. Chem.* **265**, 16035-16038.

Chap, H. J., Zwaal, R. F. and van Deenen, L. L. (1977). Action of highly purified phospholipases on blood platelets. Evidence for an asymmetric distribution of phospholipids in the surface membrane. *Biochim. Biophys. Acta* **467**, 146-164.

Cheng, J., Fujita, A., Yamamoto, H., Tatematsu, T., Kakuta, S., Obara, K., Ohsumi, Y. and Fujimoto, T. (2014). Yeast and mammalian autophagosomes exhibit distinct phosphatidylinositol 3-phosphate asymmetries. *Nat. Commun.* **5**, 3207.

Cullis, P. R. and de Kruijff, B. (1979). Lipid polymorphism and the functional roles of lipids in biological membranes. *Biochim. Biophys. Acta* **559**, 399-420.

Devaux, P. F. (1991). Static and dynamic lipid asymmetry in cell membranes. *Biochemistry* **30**, 1163-1173.

Du, G., Huang, P., Liang, B. T. and Frohman, M. A. (2004). Phospholipase D2 localizes to the plasma membrane and regulates angiotensin II receptor endocytosis. *Mol. Biol. Cell* **15**, 1024-1030.

Fujimoto, T. (1996). GPI-anchored proteins, glycosphingolipids, and sphingomyelin are sequestered to caveolae only after crosslinking. *J. Histochem. Cytochem.* **44**, 929-941.

Fujimoto, K., Umeda, M. and Fujimoto, T. (1996). Transmembrane phospholipid distribution revealed by freeze-fracture replica labeling. *J. Cell Sci.* **109**, 2453-2460.

Fujimoto, T., Kogo, H., Nomura, R. and Une, T. (2000). Isoforms of caveolin-1 and caveolar structure. *J. Cell Sci.* **113**, 3509-3517.

Fujita, A. and Fujimoto, T. (2007). Quantitative retention of membrane lipids in the freeze-fracture replica. *Histochem. Cell Biol.* **128**, 385-389.

Fujita, A., Cheng, J., Hirakawa, M., Furukawa, K., Kusunoki, S. and Fujimoto, T. (2007). Gangliosides GM1 and GM3 in the living cell membrane form clusters susceptible to cholesterol depletion and chilling. *Mol. Biol. Cell* **18**, 2112-2122.

Fujita, A., Cheng, J. and Fujimoto, T. (2009a). Segregation of GM1 and GM3 clusters in the cell membrane depends on the intact actin cytoskeleton. *Biochim. Biophys. Acta* **1791**, 388-396.

Fujita, A., Cheng, J., Tauchi-Sato, K., Takenawa, T. and Fujimoto, T. (2009b). A distinct pool of phosphatidylinositol 4,5-bisphosphate in caveolae revealed by a nanoscale labeling technique. *Proc. Natl. Acad. Sci. USA* **106**, 9256-9261.

Gordesky, S. E., Marinetti, G. V. and Segel, G. B. (1972). Differences in the reactivity of phospholipids with FDNB in normal RBC, sickle cells and RBC ghosts. *Biochem. Biophys. Res. Commun.* **47**, 1004-1009.

Haase, P. (1995). Spatial pattern analysis in eccology based on Ripley's K-function: Introduction and methods for edge correction. *J. Veg. Sci.* **6**, 575-582.

Hirota, K., Momoeda, K., Ono, K., Hanaoka, K., Horikawa, K., Okumura, K. and Iwamori, M. (1995). Alteration in the reactivity of sphingomyelin in mitogen-stimulated lymphocytes. *J. Biochem.* **118**, 4-8.

Hosoda, K., Ohya, M., Kohno, T., Maeda, T., Endo, S. and Wakamatsu, K. (1996). Structure determination of an immunopotentiator peptide, cinnamycin, complexed with lysophosphatidylethanolamine by 1H-NMR. *J. Biochem.* **119**, 226-230.

Hullin-Matsuda, F. and Kobayashi, T. (2007). Monitoring the distribution and dynamics of signaling microdomains in living cells with lipid-specific probes. *Cell. Mol. Life Sci.* **64**, 2492-2504.

Ishitsuka, R. and Kobayashi, T. (2007). Cholesterol and lipid/protein ratio control the oligomerization of a sphingomyelin-specific toxin, lysenin. *Biochemistry* **46**, 1495-1502.

Ishitsuka, R., Yamaji-Hasegawa, A., Makino, A., Hirabayashi, Y. and Kobayashi, T. (2004). A lipid-specific toxin reveals heterogeneity of sphingomyelin-containing membranes. *Biophys. J.* **86**, 296-307.

Iwabuchi, K., Prinetti, A., Sonnino, S., Mauri, L., Kobayashi, T., Ishii, K., Kaga, N., Murayama, K., Kurihara, H., Nakayama, H. et al. (2008). Involvement of very long fatty acid-containing lactosylceramide in lactosylceramide-mediated superoxide generation and migration in neutrophils. *Glycoconj. J.* **25**, 357-374.

Iwamoto, K., Hayakawa, T., Murate, M., Makino, A., Ito, K., Fujisawa, T. and Kobayashi, T. (2007). Curvature-dependent recognition of ethanolamine phospholipids by duramycin and cinnamycin. *Biophys. J.* **93**, 1608-1619.

Jacobson, K., Mouritsen, O. G. and Anderson, R. G. (2007). Lipid rafts: at a crossroad between cell biology and physics. *Nat. Cell Biol.* **9**, 7-14.

Kasahara, K., Kaneda, M., Miki, T., Iida, K., Sekino-Suzuki, N., Kawashima, I., Suzuki, H., Shimonaka, M., Arai, M., Ohno-Iwashita, Y. et al. (2013). Clot retraction is mediated by factor XIII-dependent fibrin-αIIbβ3-myosin axis in platelet sphingomyelin-rich membrane rafts. *Blood* **122**, 3340-3348.

Kiskowski, M. A., Hancock, J. F. and Kenworthy, A. K. (2009). On the use of Ripley's K-function and its derivatives to analyze domain size. *Biophys. J.* **97**, 1095-1103.

Kiyokawa, E., Makino, A., Ishii, K., Otsuka, N., Yamaji-Hasegawa, A. and Kobayashi, T. (2004). Recognition of sphingomyelin by lysenin and lysenin-related proteins. *Biochemistry* **43**, 9766-9773.

Kiyokawa, E., Baba, T., Otsuka, N., Makino, A., Ohno, S. and Kobayashi, T. (2005). Spatial and functional heterogeneity of sphingolipid-rich membrane domains. *J. Biol. Chem.* **280**, 24072-24084.

Kotani, M., Ozawa, H., Kawashima, I., Ando, S. and Tai, T. (1992). Generation of one set of monoclonal antibodies specific for a-pathway ganglio-series gangliosides. *Biochim. Biophys. Acta* **1117**, 97-103.

Larson, G. and Samuelsson, B. E. (1980). Blood group type glycosphingolipids of human cord blood erythrocytes. *J. Biochem.* **88**, 647-657.

Lillemeier, B. F., Pfeiffer, J. R., Surviladze, Z., Wilson, B. S. and Davis, M. M. (2006). Plasma membrane-associated proteins are clustered into islands attached to the cytoskeleton. *Proc. Natl. Acad. Sci. USA* **103**, 18992-18997.

Lingwood, D. and Simons, K. (2010). Lipid rafts as a membrane-organizing principle. *Science* **327**, 46-50.

Makino, A., Abe, M., Murate, M., Inaba, T., Yilmaz, N., Hullin-Matsuda, F., Kishimoto, T., Schieber, N. L., Taguchi, T., Arai, H. et al. (2015). Visualization of the heterogeneous membrane distribution of sphingomyelin associated with cytokinesis, cell polarity, and sphingolipidosis. *FASEB J.* **29**, 477-493.

Marsh, D. (2013). *Handbook of Lipid Bilayers*. Boca Raton, FL: CRC Press.

Miyazawa, A., Umeda, M., Horikoshi, T., Yanagisawa, K., Yoshioka, T. and Inoue, K. (1988). Production and characterization of monoclonal antibodies that bind to phosphatidylinositol 4,5-bisphosphate. *Mol. Immunol.* **25**, 1025-1031.

Mizuno, H., Abe, M., Dedecker, P., Makino, A., Rocha, S., Ohno-Iwashita, Y., Hofkens, J., Kobayashi, T. and Miyawaki, A. (2011). Fluorescent probes for superresolution imaging of lipid domains on the plasma membrane. *Chem. Sci.* **2**, 1548-1553.

Murate, M., Hayakawa, T., Ishii, K., Inadome, H., Greimel, P., Watanabe, M., Nagatsuka, Y., Ito, K., Ito, Y., Takahashi, H. et al. (2010). Phosphatidylglucoside forms specific lipid domains on the outer leaflet of the plasma membrane. *Biochemistry* **49**, 4732-4739.

Nagata, Y., Partridge, T. A., Matsuda, R. and Zammit, P. S. (2006). Entry of muscle satellite cells into the cell cycle requires sphingolipid signaling. *J. Cell Biol.* **174**, 245-253.

Nam, K. S., Igarashi, K., Umeda, M. and Inoue, K. (1990). Production and characterization of monoclonal antibodies that specifically bind to phosphatidylcholine. *Biochim. Biophys. Acta* **1046**, 89-96.

Ortegren, U., Karlsson, M., Blazic, N., Blomqvist, M., Nystrom, F. H., Gustavsson, J., Fredman, P. and Strålfors, P. (2004). Lipids and glycosphingolipids in caveolae and surrounding plasma membrane of primary rat adipocytes. *Eur. J. Biochem.* **271**, 2028-2036.

Perret, B., Chap, H. J. and Douste-Blazy, L. (1979). Asymmetric distribution of arachidonic acid in the plasma membrane of human platelets. A determination using purified phospholipases and a rapid method for membrane isolation. *Biochim. Biophys. Acta* **556**, 434-446.

Perry, G. L. W. (2004). SpPack: spatial point pattern analysis in Excel using Visual Basic for Applications (VBA). *Environ. Model. Softw.* **19**, 559-569.

Post, J. A., Langer, G. A., Op den Kamp, J. A. and Verkleij, A. J. (1988). Phospholipid asymmetry in cardiac sarcolemma. Analysis of intact cells and 'gas-dissected' membranes. *Biochim. Biophys. Acta* **943**, 256-266.

Prior, I. A., Muncke, C., Parton, R. G. and Hancock, J. F. (2003). Direct visualization of Ras proteins in spatially distinct cell surface microdomains. *J. Cell Biol.* **160**, 165-170.

Ramoni, C., Spadaro, F., Barletta, B., Dupuis, M. L. and Podo, F. (2004). Phosphatidylcholine-specific phospholipase C in mitogen-stimulated fibroblasts. *Exp. Cell Res.* **299**, 370-382.

Record, M., El Tamer, A., Chap, H. and Douste-Blazy, L. (1984). Evidence for a highly asymmetric arrangement of ether- and diacyl-phospholipid subclasses in the plasma membrane of Krebs II ascites cells. *Biochim. Biophys. Acta* **778**, 449-456.

Ripley, B. D. (1979). Tests of randomness for spatial point patterns. *J. R. Stat. Soc. B* **39**, 172-192.

Rothman, J. E. and Kennedy, E. P. (1977). Asymmetrical distribution of phospholipids in the membrane of Bacillus megaterium. *J. Mol. Biol.* **110**, 603-618.

Ryan, K. P., Bald, W. B., Neumann, K., Simonsberger, P., Purse, D. H. and Nicholson, D. N. (1990). Cooling rate and ice-crystal measurement in biological specimens plunged into liquid ethane, propane, and Freon 22. *J. Microsc.* **158**, 365-378.

Rzeźnicka, I. I., Sovago, M., Backus, E. H., Bonn, M., Yamada, T., Kobayashi, T. and Kawai, M. (2010). Duramycin-induced destabilization of a phosphatidylethanolamine monolayer at the air-water interface observed by vibrational sum-frequency generation spectroscopy. *Langmuir* **26**, 16055-16062.

Schick, P. K., Kurica, K. B. and Chacko, G. K. (1976). Location of phosphatidylethanolamine and phosphatidylserine in the human platelet plasma membrane. *J. Clin. Invest.* **57**, 1221-1226.

Schlaepfer, D. D., Mehlman, T., Burgess, W. H. and Haigler, H. T. (1987). Structural and functional characterization of endonexin II, a calcium- and phospholipid-binding protein. *Proc. Natl. Acad. Sci. USA* **84**, 6078-6082.

Shimada, Y., Maruya, M., Iwashita, S. and Ohno-Iwashita, Y. (2002). The C-terminal domain of perfringolysin O is an essential cholesterol-binding unit targeting to cholesterol-rich microdomains. *Eur. J. Biochem.* **269**, 6195-6203.

Sinauridze, E. I., Kireev, D. A., Popenko, N. Y., Pichugin, A. V., Panteleev, M. A., Krymskaya, O. V. and Ataullakhanov, F. I. (2007). Platelet microparticle membranes have 50- to 100-fold higher specific procoagulant activity than activated platelets. *Thromb. Haemost.* **97**, 425-434.

Takatsu, H., Tanaka, G., Segawa, K., Suzuki, J., Nagata, S., Nakayama, K. and Shin, H. W. (2014). Phospholipid flippase activities and substrate specificities of human type IV P-type ATPases localized to the plasma membrane. *J. Biol. Chem.* **289**, 33543-33556.

Tani, M. and Hannun, Y. A. (2007). Analysis of membrane topology of neutral sphingomyelinase 2. *FEBS Lett.* **581**, 1323-1328.

Thiagarajan, P. and Tait, J. F. (1991). Collagen-induced exposure of anionic phospholipid in platelets and platelet-derived microparticles. *J. Biol. Chem.* **266**, 24302-24307.

Umeda, M., Igarashi, K., Nam, K. S. and Inoue, K. (1989). Effective production of monoclonal antibodies against phosphatidylserine: stereo-specific recognition of phosphatidylserine by monoclonal antibody. *J. Immunol.* **143**, 2273-2279.

van Meer, G., Gahmberg, C. G., Op den Kamp, J. A. and van Deenen, L. L. (1981). Phospholipid distribution in human En(a-) red cell membranes which lack the major sialoglycoprotein, glycophorin A. *FEBS Lett.* **135**, 53-55.

Verkleij, A. J., Zwaal, R. F., Roelofsen, B., Comfurius, P., Kastelijn, D. and van Deenen, L. L. (1973). The asymmetric distribution of phospholipids in the human red cell membrane. A combined study using phospholipases and freeze-etch electron microscopy. *Biochim. Biophys. Acta* **323**, 178-193.

Wilson, B. S., Steinberg, S. L., Liederman, K., Pfeiffer, J. R., Surviladze, Z., Zhang, J., Samelson, L. E., Yang, L. H., Kotula, P. G. and Oliver, J. M. (2004). Markers for detergent-resistant lipid rafts occupy distinct and dynamic domains in native membranes. *Mol. Biol. Cell* **15**, 2580-2592.

Yamaji-Hasegawa, A., Makino, A., Baba, T., Senoh, Y., Kimura-Suda, H., Sato, S. B., Terada, N., Ohno, S., Kiyokawa, E., Umeda, M. et al. (2003). Oligomerization and pore formation of a sphingomyelin-specific toxin, lysenin. *J. Biol. Chem.* **278**, 22762-22770.

Yeung, T., Gilbert, G. E., Shi, J., Silvius, J., Kapus, A. and Grinstein, S. (2008). Membrane phosphatidylserine regulates surface charge and protein localization. *Science* **319**, 210-213.

Yeung, T., Heit, B., Dubuisson, J. F., Fairn, G. D., Chiu, B., Inman, R., Kapus, A., Swanson, M. and Grinstein, S. (2009). Contribution of phosphatidylserine to membrane surface charge and protein targeting during phagosome maturation. *J. Cell Biol.* **185**, 917-928.

Yilmaz, N., Yamada, T., Greimel, P., Uchihashi, T., Ando, T. and Kobayashi, T. (2013). Real-time visualization of assembling of a sphingomyelin-specific toxin on planar lipid membranes. *Biophys. J.* **105**, 1397-1405.

Zachowski, A. (1993). Phospholipids in animal eukaryotic membranes: transverse asymmetry and movement. *Biochem. J.* **294**, 1-14.

Journal of Cell Science